Science of Sintering, **39** (2007) 133-144

doi:10.2298/SOS0702134Y

UDK 622.785:666.112.2:661.183.8

Integrated Liquid-Phase Sintering of Glass-Alumina Functionally Graded Materials

C. L. Yu*, X. F. Wang, X. Tong, H. T. Jiang, G. W. Wang
School of Materials Science and Engineering, Shaanxi University of Science & Technology, Xi'an 710021, P. R. China

Abstract:

The sintering mechanism of glass-alumina functionally graded materials (G-A FGMs) at 710℃ prepared by a novel rapid prototyping manufacturing (RP&M) technology was studied. An integrated kinetics equation was established for the initial 20 minutes. Linear shrinkage is due to the integrated working of both viscous flow of the glass particles and gravitation of the effective activated alumina grain boundaries towards the equilibrium state. The driving force for gravitation of the activated alumina grain boundaries originates from the coactions of passive flow of the alumina particles during viscous flow of the glass particles and the compressive stress formed during cooling. In the middle 10 minutes, the sintering process follows the solution-precipitation mechanism. Confirmed by Scanning Electron Microscope (SEM) and the line scanning Energy Dispersive Spectrum (EDS), a layer of Si-Al eutectic of about 1.04μm on the alumina surface is formed. Then the alkali and alkali earth ions in the glass phase diffuse through this layer and precipitate on the surface. Additionally, the dissolved Al ions can easily transport through the eutectic layer and precipitate in the glass matrix due to the effect of Si in the glass matrix.

Keywords: *Liquid-phase sintering; Glass; Alumina; Functionally graded materials; Activated grain boundaries*

Introduction

Functionally graded materials (FGMs) are newly developed multi-phase systems intended to limit ambient circumstances, for instance, circumstances with extraordinary high temperature or great thermal shock [1]. Differing from common composites, the composition and/or microstructure is not uniform in space, but varies following a pre-determined profile, which yields a spatial gradient of material properties and functions [2]. In most cases, FGMs are characterized by spatial gradient variation of one ingredient material in another. For example, metal with higher strength and toughness and ceramics with higher temperature resistance and/or corrosion resistance are combined together by a heterogeneous transition structure with near-continuously gradient variation of both materials [3]. If properly designed, the introduction of a smooth variation may significantly reduce the large-scale stress singularities, which usually arise at sharp interfaces between heterogeneous materials such as metallic and ceramic materials [4]. FGMs have been currently used in aerospace industry,

*) Corresponding author: yucl1226@tom.com

energy industry, and biomedical engineering, especially when the thermo-mechanical loading conditions are not uniform and the gradient of microstructure and related properties can be tailored to the service requirements [5, 6].

Up to now, most FGMs contain at least one metallic phase and the FGMs composed of glass and ceramics have not been systematically studied. In 2006, Cannillo and his co-workers proposed a method of percolating the molten CaO-ZrO_2-SiO_2 glass into the polycrystalline sintered alumina substrate to prepare glass-alumina functionally graded materials (G-A FGMs) and effects of sintering temperature and time on the penetration depth were studied [7, 8]. In addition, the crack propagation of the prepared G-A FGMs was also simulated by coupling the finite element method with the Griffith theory [9].

Previous research has shown that the preparation technology is one of the critical factors to enhance the properties of high-performance FGMs. However, it is still difficult to produce complex transition structures by interpenetrating, interweaving, and connecting. Thus, new preparation technologies and relevant facilities have been focused on for FGMs [10-14]. Among the optimal technologies, rapid prototyping manufacturing (RP&M) technology [15], an efficient computerized fabrication technology that can produce complex components with a locally controlled composition and structure, offers a good potential to fabricate irregular 3-D FGMs [16].

Recently, G-A FGMs using Na_2O-CaO-SiO_2 glass and polycrystalline alumina as ingredient materials based on a new RP&M technology, have been prepared by our research group [17-19] (Fig. 1). In the previous work [19], sintering properties of the G-A FGMs were analyzed and effects of the sintering temperature and time on flexural strength and water absorption rate were discussed.

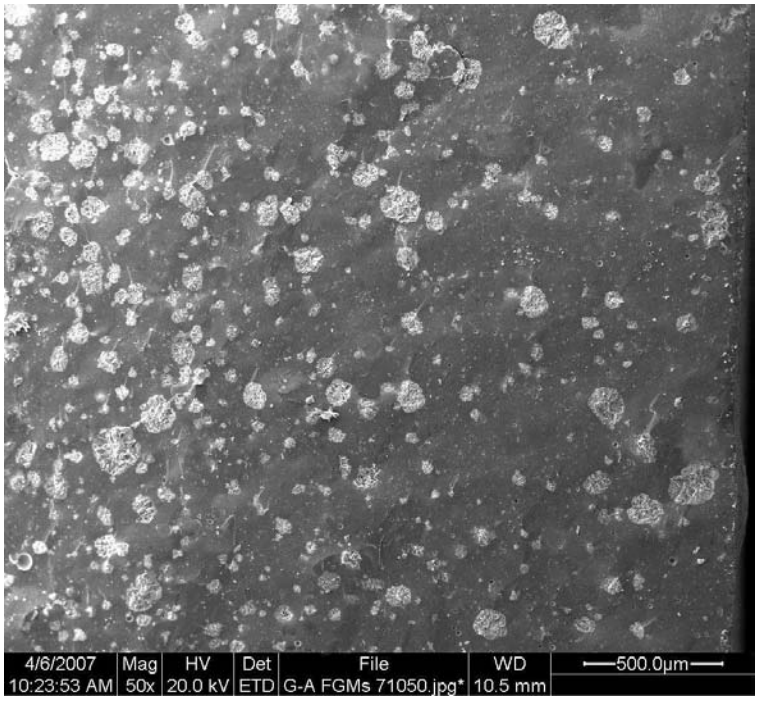

Fig. 1 Micrograph of the G-A FGMs at 710°C for 50 minutes; the spatial gradient distribution of alumina in glass matrix can be clearly seen from left to right

It was found that the sintering process of the G-A FGMs did not follow the pure liquid-phase sintering mechanism, but was characterized by a so-called integrated sintering

mechanism, which had a great effect on the microstructure and other properties. This present work intends to establish the kinetics equation of the integrated liquid-phase sintering process and to investigate the mass transport process during sintering of the G-A FGMs.

2. Experimental procedure

The fine Na_2O-CaO-SiO_2 glass powders were prepared by ball-milling of Na_2O-CaO-SiO_2 granulations, which were obtained by quenching Na_2O-CaO-SiO_2 melts at 1200°C in cold water. The analytic reagent polycrystalline alumina powders were obtained from the Xi'an Chemical Reagent Plant, China. Both the glass and alumina powders were filtered by a 400-mesh cloth. Freeform fabrication of the G-A FGMs was conducted by the equipment produced by our research group [19] and the fabrication process was accurately described in our previous work [18, 19]. The relevant properties of the ingredient materials are summarized in Tab. I.

Tab. I Properties of the ingredient materials

Ingredient materials	Young's modulus (GPa)	Poisson ratio	Thermal expansion coefficient (°C^{-1})
Glass	69	0.25	9.0×10^{-6}
Alumina	366	0.20	8.3×10^{-6}

According to the previous research [20], heat treatment of the dried G-A FGMs body was conducted at a temperature rising velocity of 5°C/min from room temperature to 260°C, and a subsequent 2°C/min from 260°C to 280°C, and preserved at 280°C for 4 hours to burn out the organic binders. The body was finally sintered at 710°C for different times and quickly cooled to get G-A FGMs. For the data processing of the linear shrinkage, the average value of 10 identical samples was determined as the final value for each experimental condition. The standard deviation for each group of data was less than 2%.

Microstructure of the cross sections was observed with Environmental Scanning Electron Microscopy (ESEM, Quanta 200, Philips-FEI Cooperation, Holland) and the line scanning Energy Dispersive Spectrum (EDS) of the elements in the boundary areas between glass and alumina were obtained by the same equipment.

3 Results and discussion

According to the general equation proposed by Woolfrey and Bannister [21], the kinetics equation for the isothermal sintering process is expressed by

$$\frac{d}{dt}\left(\frac{\Delta L}{L_0}\right) = A_0 \exp\left(-\frac{Q}{RT}\right)/(\Delta L / L_0)^m \qquad (1)$$

where $\Delta L/L_0$ is the relative linear shrinkage, t is the sintering time, A_0 is a constant depending only on the material parameters and sintering mechanism, and m has different values depending on the dominant mass transport mechanism.

At fixed temperature, eq. (1) can be transformed into eq. (2) by integration,

$$\left(\frac{\Delta L}{L_0}\right)^{m+1} = Kt \qquad (2)$$

where K is a constant equal to $(m+1)A_0 \exp\left(-\frac{Q}{RT}\right)$.

In logarithmic form,

$$(m+1)\ln\left(\frac{\Delta L}{L_0}\right) = \ln K + \ln t \qquad (3)$$

Linear fit results of the data according to eq. (3) are shown in Fig. 2 in which three typical periods are exhibited for the relationship between ln($\Delta L/L_0$) and ln$t$. The parameters, corresponding values and errors are summarized in Tab. II. As depicted in Fig. 2 and Tab. II, 1/(m+1) is equal to 2.4452 with a maximum error of ±0.0532, resulting in the fact that m is less than 0.

Tab. II Parameters, values and errors for the linear fit

Period	**arameter**	**alue**	**rror**	
(a)	A	-9.45029	0.12293	0.99813
	B	2.4552	0.0532	
(b)	A	-3.01565	0.00794	0.99987
	B	0.30902	0.00247	
(c)	A	-2.12921	0.05683	0.95143
	B	0.04781	0.01547	

Note: the mathematical model employed is Y=A+B*X in which A, B are equal to ln$K$/(m+1) and 1/(m+1) in eq. (1) respectively.

It is not consistent with the simple equation of time dependent linear shrinkage proposed by Frenkel [22]. However, it is undoubtedly because the viscous flow of the glass particles contributes to the linear shrinkage during liquid-phase sintering, as the boundary areas between the glass particles have been filled with a certain amount of liquid phase at 710°C even for several minutes, which can be confirmed by SEM. Thus, the linear shrinkage of the G-A FGMs is not simply owing to the viscous flow of the glass particles but also to the coactions of both the ingredient materials.

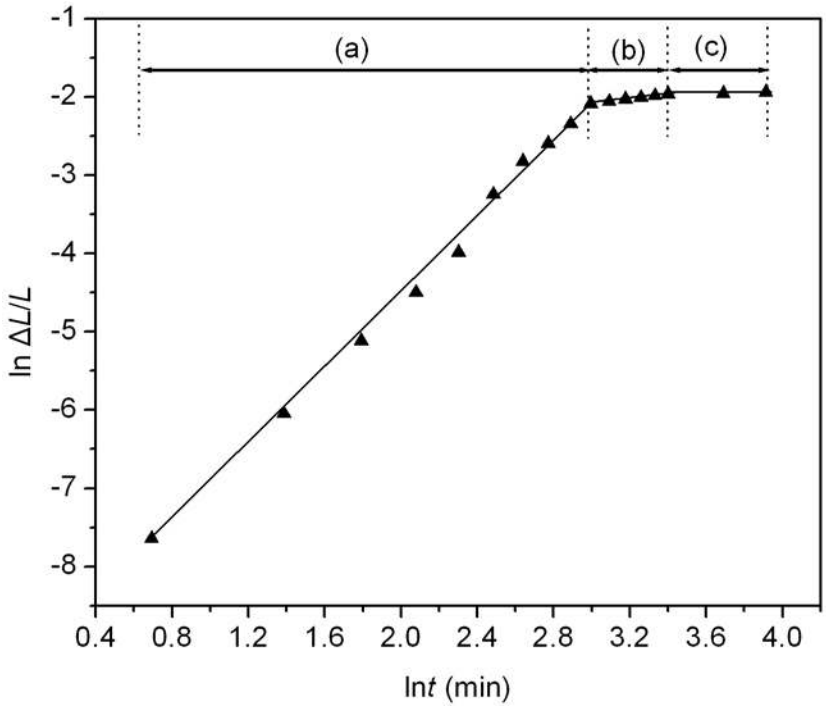

Fig. 2 ln($\Delta L/L_0$) vs. ln$t$ curve for the G-A FGMs at 710°C

As shown in Fig. 1, the local structures of G-A FGMs can be regarded as composite materials in which alumina particles are encapsulated by the glass matrix. The morphology of the raw alumina powders is shown in Fig. 3. It is obvious that these powders are irregular shaped and an uncompacted contact will be formed between the powders when two or more are encapsulated together by the glass matrix, resulting in weak bonding between the alumina grains. Fig. 4 shows the microstructure of the alumina particles encapsulated by the glass matrix in the G-A FGMs at 710°C for 50 minutes. Although close bonding is exhibited in the boundary area between glass and alumina, large numbers of cavities and dislocations are distributed along the grain boundaries in the alumina particles. We define these weakly bonded alumina grain boundaries as activated ones because they will contribute to the shrinkage of the G-A FGMs as well [23]. In accordance with reference [24], the effective activated volume of these alumina grain boundaries is defined as

$$v = -RT\left(\frac{\partial \ln D}{\partial p}\right) \tag{4}$$

where the diffusion coefficient D is defined as

$$D = \gamma a^2 v \exp\left(-\frac{\Delta G}{RT}\right) \tag{5}$$

and R is the gas constant, T is the sintering temperature, ΔG is the change in free energy, p is the pressure, γ is the geometric factor, a is a crystal lattice constant, and v is the Debey frequency.

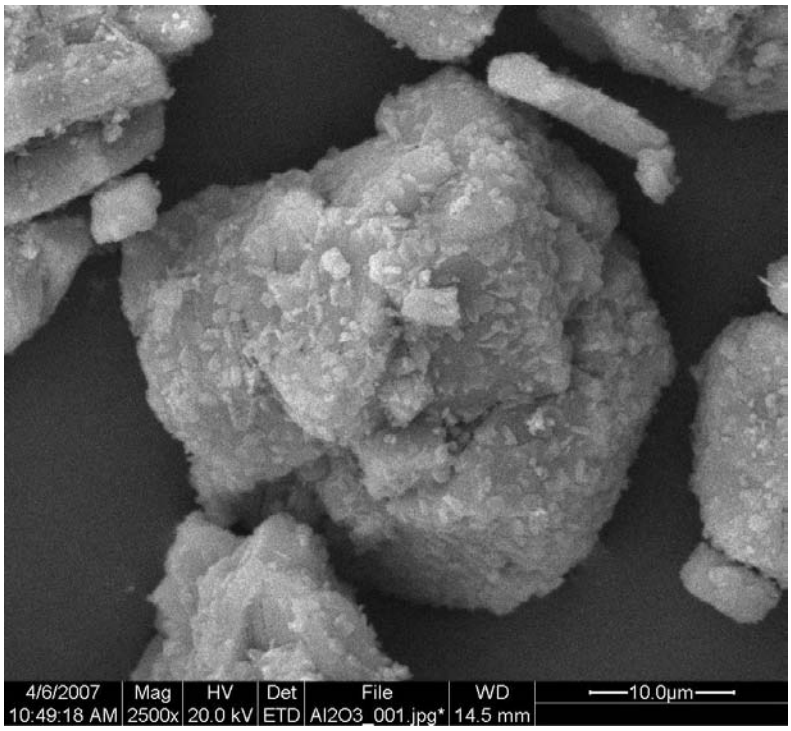

Fig. 3 Morphology of the ingredient material alumina powders

At the onset of sintering, a system is characterized by a starting effective activated volume v^0. From the viewpoint of processes occurring during sintering, it can be described as gravitation of the electronic system towards an equilibrium state [23]. The equilibrium state of the system can be characterized by the equilibrium activated volume v^+. The effective activated volume v of a system at any moment during the sintering process is a parameter that,

with the increase of sintering time, gravitates towards the equilibrium activated volume.

From a physical viewpoint the effective activated volume of a system can be defined as

$$v = \frac{N_0}{N_r} v^+ \tag{6}$$

where N_0 represents the concentration of all defects at any given moment and N_r represents the equilibrium concentration of defects in the analyzed system.

According to reference [25] reduction of the effective activated volume can be simply defined as

$$\frac{v}{v^+} = 1 + (\frac{v^0}{v^+} - 1)\exp(-t) \tag{7}$$

For G-A FGMs, in the most general sense, kinetics of the sintering process can be expressed in terms of the dependence of linear shrinkage during isothermal sintering on the sintering time [23] as

$$\frac{\Delta L}{L_0} = Kt^n \tag{8}$$

where K is the sintering rate constant which depends on the sintering temperature and time, n is a constant which depends on the process mechanism, and t is the sintering time. The sintering rate constant is defined as

$$K = K_0 \exp(-\frac{E}{RT}) \cdot \varphi(t) \tag{9}$$

where K_0 is a constant, R is the gas constant, E is the process activation energy, and T is the sintering temperature. The parameter $\varphi(t)$ represents a measure of the degree of sintering. If sintering is viewed as the consequence of reduction of the activated alumina grain boundaries, then the degree of sintering can be defined as the ratio between the equilibrium activated volume and the effective activated volume,

$$\varphi(t) = \frac{v^+}{v} \tag{10}$$

then taking into account eq. (7) we obtain

$$\varphi(t) = \frac{1}{1 + C\exp(-t)} \tag{11}$$

where C is a constant defining the ratio between the starting effective activated volume and the equilibrium activated volume of alumina grain boundaries.

Thus the following equation can be used to describe the sintering kinetics,

$$\frac{\Delta L}{L_0} = \frac{K}{1 + C\exp(-t)} \cdot t^n \tag{12}$$

Considering the viscous flow of glass particles and the reduction of the effective activated alumina grain boundaries taking place at the same time during isothermal sintering, then an integrated kinetics equation for period (a) can be expressed as

$$\frac{\Delta L}{L_0} = K_1 t + \frac{K_2}{1 + C\exp(-t)} \cdot t^n \tag{13}$$

The non-linear fit of the data according to eq. (13) and the values and errors of the parameters are shown in Fig. 5. A square of the correlation coefficient R of 0.99097 is determined indicating the proper adoption of eq. (13).

The coefficient K_1 for the first part right of the equal sign in eq. (13) is 0.00013 determining the importance of the viscous flow of the glass particles which mainly takes place at 710°C because no obvious compaction of glass particles is identified before it.

According to Frenkel's theory [22], the sintering process concerning the viscous flow of the glass particles takes place in two stages. In the first stage, the glass particles combine during which the contact surface between particles increases; which in the end results in forming pores in the system. In the second stage, the process of pores overrun takes place. That's when pores, representing an infinitely huge concentration of vacancies, decrease due to diffusion through glass. However, decrease of the volume of pores will stop when the pressure becomes equal to the capillary pressure. And, if a liquid phase is formed in the contact areas due to the produced local stress [26], the decrease will stop immediately even if the pressure is less than the capillary pressure.

In addition, the chosen Na_2O-CaO-SiO_2 glass can form well moistened with alumina, which is essential to the well bonding of the two materials; as shown in Fig. 4. The well bonding is owing to the capillaries formed between alumina particles and a large capillary force which will be formed, causing the liquid glass phase to penetrate into them. This is due to the well bonding which encapsulated alumina particles flow together with the glass particles, which also contributes to the shrinkage of the G-A FGMs.

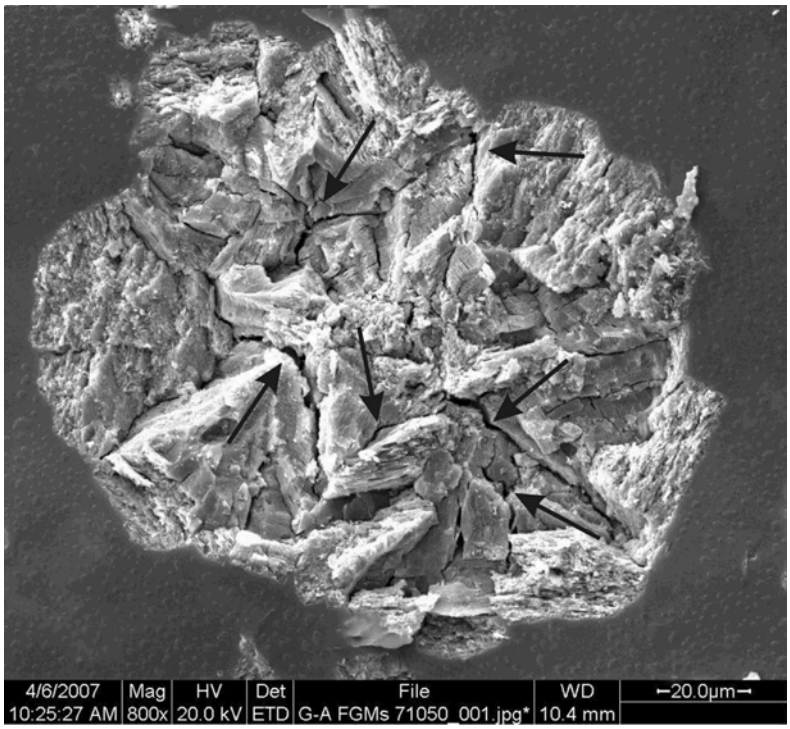

Fig. 4 Micrograph of the alumina particles encapsulated by the glass matrix; the black arrows demonstrate the residual cavities in the alumina after fracture

The calculated value of *C* in the second part right of the equal sign in eq. (13) is 1.30428 which indicates that the starting effective activated volume of alumina grain boundaries is 2.3 times greater than the equilibrium one. This is partially due to the passive flow of alumina particles as some of the cavities or dislocations will disappear during the relative motion of the particles. On the other hand, compressive stress will be formed in the surface layer of the alumina particles during rapid cooling due to the working of the glass matrix as its thermal expansion coefficient is larger than that of the alumina (see Tab. I). From the measured compressive stress in the G-A FGMs by Cannillo using CaO-ZrO_2-SiO_2 glass and polycrystalline alumina with thermal expansion coefficients of 8.7×10^{-6}°$C^{-1}$and 8.2×10^{-6}°C^{-1} respectively, it was determined that the maximum compressive stress in the FGMs was -

8MPa [27]. As demonstrated by the microstructure in Fig. 4, it can be inferred that these cavities or dislocations will decrease or disappear during cooling when compressive stress is formed. This is due to the passive flow of the alumina particles and the compressive stress formed in the surface layer during cooling in which the effective alumina grain boundaries gravitate towards the equilibrium state.

The gravitation process mainly takes place at 710°C which is demonstrated by the observation that no obvious compaction for alumina is formed before it. Only weak mechanical contact between alumina particles is formed before 690°C (the softening temperature of the chosen glass). This is determined by the freeform fabrication process as no external forces are applied. And, no obvious compaction is found from 690°C to 710°C confirmed by SEM due to the fact that no moistening is formed between glass and alumina. On the other hand, it takes only 4 minutes from 690°C to 710°C at a temperature rising velocity of 5°C/min, which is rather short compared with the sintering process at 710°C.

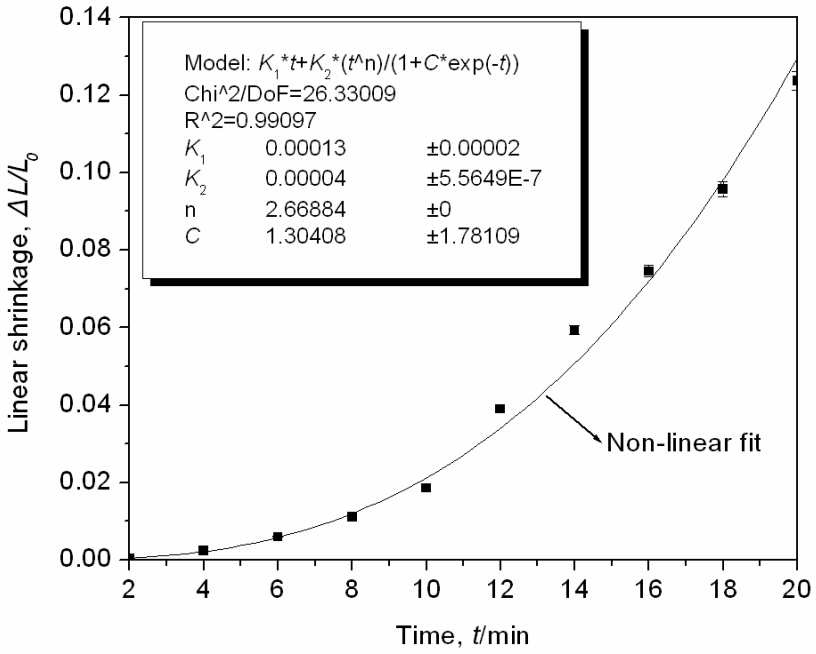

Fig. 5 Non-linear fit of the linear shrinkage as a function of sintering time; the data are trained with a Levenberg-Marquardt algorithm for about 200 epochs**.**

From Fig. 2 and Tab. II, the slope coefficient of period (b) which lasts for about 10 minutes changes into 0.31, which is in good agreement with the solution-precipitation mechanism of liquid-phase sintering proposed by Kingery [26]. According to Kingery's theory, the solubility of alumina in the liquid glass phase is greater than that in the free surface, causing the mass transport of Al through the liquid phase in the boundary area and precipitation in the glass matrix. However, from line scanning EDS of the elements in the boundary area, the real mass transport process does not obey this principle, but follows a more complicated one.

The boundary area between alumina and glass is shown in Fig. 6 and the line scanning EDS of the elements along line section AB is given in Fig. 7. The total distance of line section AB is about 4.4μm. From the overall energy dispersive spectrums of Na, Ca, O, Si, and Al elements along line section AB, section AC of about 0.4μm is determined to be the pure alumina since no alkali and alkali earth ions are detected. The detected energy of Al

decreases gradually from point C till point D, but increases sharply from point D to point E. In accordance with the EDS of Al, strong energy of Si is also detected along section DE of about 1.04μm.

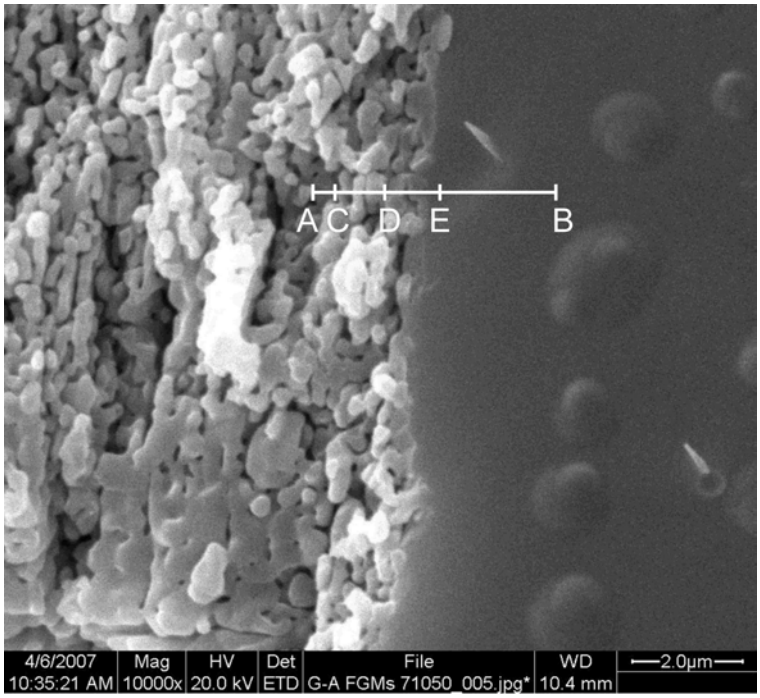

Fig. 6 Micrograph of the boundary of the alumina and glass; the line scanning EDS is conducted along line section AB

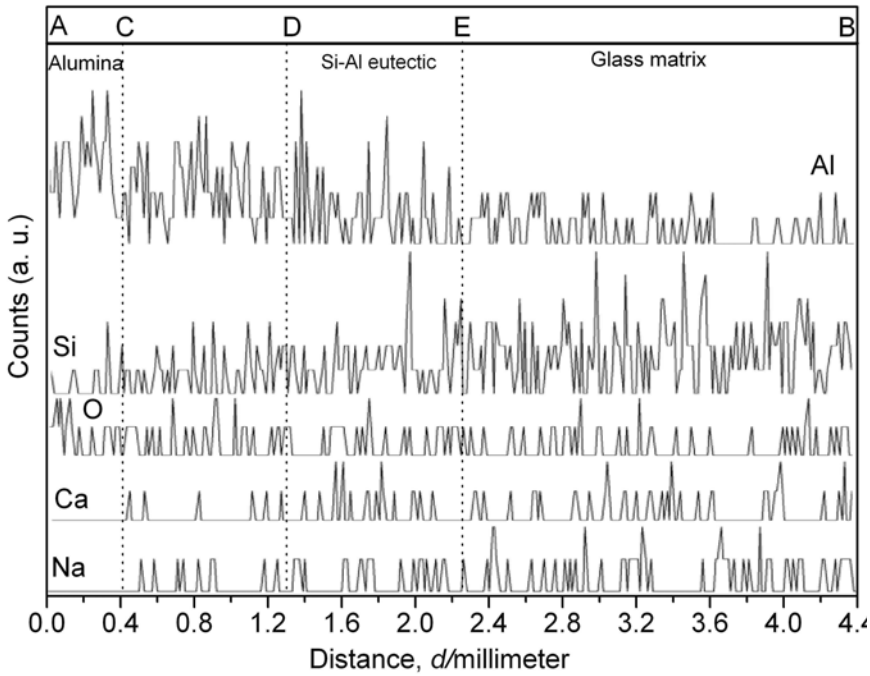

Fig. 7 Line scanning energy dispersive spectrums of Na, Ca, O, Si and Al elements along line section AB in fig. 6

However, the detected energy of Si along section AD right to section DE is relatively weak so that section DE is determined to be a layer rich in Al and Si possibly due to the formation of Si-Al eutectic [28]. From Savitskii's theory, the transport of all the elements can be clearly interpreted. In the initial stage, the Si ions transport to the alumina surface to form a layer of Si-Al eutectic of about 1.04μm with the Al ions. Such an event is the consequence of the phase transition caused by lowering the melting temperature of the layer when its chemical composition has changed [29]. Then the Na and Ca ions in the glass diffuse through this layer and precipitate along section CD of about 0.9μm. Due to the large diffusing resistance, a majority of the Ca ions precipitate in the eutectic layer. Moreover, further dissolution of Al in the eutectic layer can be confirmed by the relatively lower detected energy of Al along section CD. The dissolved Al will transport through the eutectic layer and precipitate in the glass matrix, which can be confirmed by the existing energy dispersive spectrum of Al along section EB. In our opinion, the EDS of Si and Al along section AD and EB are due to the combined action of both the elements.

For period (c) in Fig. 2, the slope coefficient is 0.05, indicating the densification rate is rather slow compared with period (a) and period (b). In this period, the mass transport is difficult due to the high viscosity of the glass. This period lasts for 20 minutes which also suggests the difficulty of mass transport.

4. Conclusions

The sintering mechanism of the glass-alumina functionally graded materials at 710°C prepared by a novel rapid prototyping manufacturing technology is studied. An integrated kinetics equation is established for the initial 20 minutes and the linear shrinkage is due to the integrated working of both viscous flow of the glass particles and gravitation of the effective activated alumina grain boundaries towards the equilibrium state. The driving force for gravitation of the activated alumina grain boundaries comes from the coactions of the passive flow of the alumina particles and the compressive stress formed during cooling. In the middle 10 minutes, the sintering process follows the solution-precipitation mechanism. Confirmed by SEM and the line scanning EDS, a layer of Si-Al eutectic of about 1.04μm on the alumina surface was formed. Then the alkali and alkali earth ions in the glass phase diffuse through this layer and precipitate in the surface of the alumina particles. Additionally, the dissolved Al ions can easily transport through the eutectic layer and precipitate in the glass matrix due to the effect of Si in the glass.

Acknowledgement

This work was supported by the Natural Science Funds of Shaanxi Province, P. R. China (Granted No. 2000C35).

References

1. Y. Miyamoto, W. A. Kaysser, B. H. Rabin, A. Kawasaki, R. G. Ford, Functionally Graded Materials. Design, Processing and Applications, Kluwer Academic Publishers, 1999.
2. A. Kawasaki, R. Watanabe, Ceram. Int., 23(1997), 73.
3. J. S. Xiao, B. Jiang, J. Liu, S. Y. Huang, Journal of Wuhan University of Technology, Materials Science Edition, 18, (2003), 38.

4. T. L. Becker, R. M. Cannon, R. O. Ritchie, Eng. Fract. Mech., 69(2002), 1521.
5. C. E. Rousseau, H. V. Tippur, Int. J. Fract., 114(2002), 87.
6. L. Librescu, S. Y. Oh, O. Song, Journal of Thermal Stresses, 28, (2005), 649.
7. V. Cannillo, T. Manfredini, C. Siligardi, A. Sola, J. Eur. Ceram. Soc., 26, (2006), 993.
8. V. Cannillo, T. Manfredini, C. Siligardi, A. Sola, J. Eur. Ceram. Soc., 26, (2006), 2685.
9. V. Cannillo, T. Manfredini, M. Montorsi, C. Siligardi, A. Sola, J. Eur. Ceram. Soc., 26, (2006), 3067.
10. Y. Miyamoto, Materials Science Research International, 6, (2000), 3.
11. Z. Y. Zhao, J. C. Fang, H. Y. Li, Transactions of Nonferrous Metals Society of China (English Edition), 15, (2005), 427.
12. G. Zeng, Z. D. Yin, J. C. Zhu, M. W. Li, Journal of Materials Science and Technology, 19, (2003), 63.
13. C. W. Park, Industrial and Engineering Chemistry Research, 9, (2000), 79.
14. N. Bertolino, M. Monagheddu, A. Tacca, P. Giuliani, C. Zanotti, F. Maglia, T. U. Anselmi, Journal of Materials Research, 18, (2003), 448.
15. X. F. Wang, H. J. Luo, Rapid Prototyping Manufacturing Technology, China Light Industry Press, Beijing, 2001.
16. Y. M. Zhang, J. C. Han, X. H. Zhang, X. D. He, Z. Q. Li, Y. D. Shan, Mat. Sci. Eng. A0: Structural Materials: Properties, Microstructure and Processing, 299, (2001), 218.
17. C. L. Yu, X. F. Wang, H. T. Jiang, L. J. Shan, A rapid fabrication method for ceramic parts, China patent application No. CN200510043174, 2005.
18. C. L. Yu, X. F. Wang, H. T. Jiang, L. J. Shan, Materials for Mechanical Engineering, 30, (2006), 28 (in Chinese).
19. C. L. Yu, X. F. Wang, H. T. Jiang, X. Tong, W. L. Yang, Rapid fabrication and sintering properties of glass-alumina functionally graded materials, in: "The Proceedings of the China Association for Science and Technology: Vol. 3.", Eds. C. G. Feng, et al., Science Press USA Inc., 2006, pp. 42-47.
20. C. L. Yu, X. F. Wang, H. T. Jiang, L. J. Shan, Electronic Components and Materials, 25, (2006), 36 (in Chinese).
21. J. L. Woolfrey, M. J. Bannister, J. Am. Ceram. Soc., 55, (1972) 390.
22. M. M. Ristić, S. Dj. Milosević, Sci. Sintering, 38, (2006), 7.
23. M. V. Nikolić, N. Labus, M. M. Ristić, Sci. Sintering, 37, (2005), 19.
24. M. M. Ristić, Kinetics of the sintering process from the viewpoint of a thermodynamic formulation of mass transport, Glas CCXCV, Serbian Academy of Sciences and Arts, Department of Technical Sciences, vol. 11, 1976 (in Serbian).
25. C. P. Flynn, Point Defects and Diffusion, Clarendon Press, Oxford Press, Oxford, 1972.
26. W. D. Kingery, H. K. Bowen, D. R. Uhlmann, Introduction to Ceramics (2nd Edition), John Wiley and Sons, New York, 1976.
27. V. Cannillo, M. Montorsi, C. Siligardi, A. Sola, G. de Portu, L. Micele, G. Pezzotti, J. Eur. Ceram. Soc., 26, (2006), 1411.
28. J. Schneider, J. Klein, M. Muske, K. Hübener, S. Gall, W. Fuhs, Aluminium-induced crystallization of amorphous silicon: Interface influence on grain growth, in: "19th European Photovoltaic Solar Energy Conference", Paris, France, 2004, pp. 7-11.
29. A. P. Savitskii, Sci. Sintering, 37, (2005), 03.

Садржај: *Проучен је механизам синтеровања функционално градираних материјала стакла-алумине (G-A FGMs) на припремљених на 710°C новом технологијом прављења прототипова (RP&M). Одређена је интегрисана кинеточка једначина за првих 20 минута. Линеарно скупљање се одвија услед интегрисане акривности вискозног тока честица стакла и гравитацијом ефектиних активираних граница зрна алумине ка равнотежном стању. Покретачка сила гравитације активираних граница зрна алумине води порекло од заједничког дејства пасивног тола честица алумине током вискозног тока честица стакла и компресивне силе која се формира током хлађења. У средњих 10 минута процес синтеровања прати механизам растварања-преципитације. Скенирајућа електронска микроскопија (СЕМ) и линијски скенирајући енергетски дисперзан спектар (ЕДС) су потврдили формирање слоја Si-Al еутектике од око 1.04μm на површини алумине. Додатно, растворени јони Al се лако транспортују кроз еутектички слој и преципитирају на стакленој матрици услед ефекта Si у стакленој матрици.*

Кључне речи: *Синтеровање у присуству течне фазе, стакло, алумина, функционално градирани материјали, активиране границе зрна.*